

Topical Review

Carbon-based perovskite solar cells with electron and hole-transporting/-blocking layers

Wenjin Yu^{1,3} , Yu Zou^{1,3} , Shining Zhang², Zishi Liu¹, Cuncun Wu^{2,*} , Bo Qu¹, Zhijian Chen¹ and Lixin Xiao^{1,*} 

¹ State Key Laboratory for Artificial Microstructure and Mesoscopic Physics, Department of Physics, Peking University, Beijing 100871, People's Republic of China

² School of Materials Science and Engineering, Hebei University of Technology, Tianjin 300130, People's Republic of China

E-mail: cuncunwu@163.com and lxxiao@pku.edu.cn

Received 31 December 2022, revised 4 February 2023

Accepted for publication 14 February 2023

Published 15 March 2023



Abstract

Towards commercialization of perovskite solar cells (PSCs), further reducing the cost and increasing the stability of PSCs have been the most important tasks of researchers, as the efficiency of single-junction PSCs has reached a competitive level among all kinds of single-junction solar cells. Carbon-electrode-based PSCs (CPSCs), as one of the most promising constructions for achieving stable economical PSCs, now attract enormous attention for their cost-effectiveness and stability. Here, we briefly review the development of CPSCs and reveal the importance of n-i-p architecture for state-of-the-art CPSCs. However, despite their promising potential, challenges still exist in CPSCs in the n-i-p architecture, which mainly stem from the incompact contact of the hole-transporting layer (HTL)/carbon electrode. Thus, new carbon materials and/or novel manufacturing methods should be proposed. In addition, HTL is yet to be appropriate for state-of-the-art CPSCs because the fabrication of carbon electrode could result in the destruction of the underlayer. To further enhance the performance of CPSCs, both the HTL and electron transport layer as well as their interfaces with perovskite active layer need to be improved. We recommend that the perovskite active layer, with its long carrier lifetime, strong carrier transport capability, and long-term stability, is necessary as well for improved performance of CPSCs. We also highlight current researches on CPSCs and provide a systematic review of various types of regulation tools.

Keywords: carbon-electrode-based PSCs, n-i-p architecture, electron transport layer, hole-transporting layer, interface

³ Co-first authors.

* Authors to whom any correspondence should be addressed.



Original content from this work may be used under the terms of the [Creative Commons Attribution 4.0 licence](https://creativecommons.org/licenses/by/4.0/). Any further distribution of this work must maintain attribution to the author(s) and the title of the work, journal citation and DOI.

Future perspectives

Towards commercialization of perovskite solar cells (PSCs), further reducing the cost and increasing the stability of PSCs are necessary. Carbon-electrode-based PSC (CPSC) is a crucial candidate for further development of a flexible, low-cost, stable, large-scale module, as the technique is compatible with the developed roll-to-roll manufacturing process. Despite their promising potential, present techniques involving carbon electrode for efficient n-i-p architecture are not yet appropriate. The main challenge stems from the destruction of the underlayer during the fabrication of carbon electrode. Future research into finding a new and appropriate carbon electrode and a chemically-stable hole-transporting layer (HTL) will play a key role in the development of advanced CPSCs. For carbon-electrode research, new carbon precursor materials and new deposition methods are anticipated. Meanwhile, for HTL research, chemically stable inorganic materials, such as CuSCN and Cu_xS_y, are promising candidates. Future studies into the long-term stability of CPSCs and its influencing factors are essential, while the matching encapsulation technology also awaits further improvement.

1. Introduction

Perovskite solar cell (PSC) has been one of the most promising photovoltaic technologies because of its low-cost large-scale manufacturing process and inspiring photovoltaic performance, with power conversion efficiency (PCE) over 25% [1–4]. Towards commercialization of PSCs, further reducing the cost and increasing the stability are necessary. Due to the high chemical reactivity of the metal halide perovskite, even the inert noble metal electrodes, such as Au and Ag, cannot survive [5, 6]. Carbon electrodes, one of the most promising substitutions, now attract more and more attention (figure 1(a)) for their low cost and potential stability. They also fit in well with the manufacturing of large-scale and flexible PSCs, which commercialization asks for. Rapid progress of carbon-electrode-based PSC (CPSC) has been achieved in recent years, as shown in figure 1(b).

In 1996, Kay and Grätzel first reported a dye-sensitized solar cell with a promising PCE of 6.7%, using graphite/carbon black composite pastes [7]. As for the PSC applications, in 2013, Han *et al* first reported a full printable processed PSC with carbon electrode (figure 1(c) (i)) [8]. Since then, CPSCs became one of the focus tasks in PSC research field. Before 2016, all researchers focused on hole-transporting-layer (HTL)-free devices (figure 1(c) (ii)), as the solvent of carbon pastes can dissolve the commonly used HTL 2,2',7,7'-tetrakis[N, N-di(4-methoxyphenyl)amino]-9,9'-spirobifluorene (Spiro-OMeTAD), and perovskite can transport holes well itself [9]. However, the efficiencies of CPSCs based on this HTL-free architecture were restricted for inefficient charge collecting by interfacial energy barriers, and thus open-circuit voltage V_{OC} loss. Besides, the commercialization of CPSCs with this architecture suffered from the high-temperature process of mesoporous TiO₂ fabrication.

In 2016, researchers published complete n-i-p architectures by using alternative HTL (figure 1(c) (iii)), such as copper(II)

phthalocyanine (CuPc) [10]. Since the mismatch of energy level and the poor contact at 6,6-phenyl C₆₁-butyric acid methyl ester (PCBM)/carbon-electrode interface, it had long been a challenge for achieving CPSC with p-i-n architectures (figure 1(c) (iv)). In 2017, Jeon *et al* achieved the p-i-n architecture by mechanically transferring the prefabricated carbon nanotubes as electrodes [11]. We propose the n-i-p architecture for state-of-the-art CPSCs to achieve appropriate energy level of carbon electrode for hole extraction and transport.

In recent years, CPSCs have made great progress, with PCE as high as 22.07% [12], approaching that of metal electrode PSCs and possessing excellent operational stability. In addition to the most commonly used commercial carbon pastes, a variety of carbon-electrode materials have been developed over the past few years for CPSCs, including carbon nanotubes [12], carbon black [13, 14], and graphene [15]. The emergence of these new carbon electrodes has also liberated the use of HTL commonly used in high-efficiency metal PSCs, such as Spiro-OMeTAD, which has led to a major advancement in the PCE of CPSCs. However, the high cost and complicated process of special carbon-electrode materials and the poor stability of the traditional HTL Spiro-OMeTAD are not fully compatible with the original intention of developing CPSCs that are low cost, stable, and suitable for large-scale commercial manufacturing, while there are still gaps in the PCE of CPSCs fabricated by traditional inexpensive carbon paste. Challenges come from the defects of each functional layer, as well as the delays and obstacles of charge transport and transfer kinetics due to the intrinsic poor conductivity of carbon electrodes and the interfacial defects. Therefore, optimization at the perovskite layer, transporting layer/blocking layer, electrode, and interfaces is essential for the improvement of the overall device performance.

Herein, we highlight the current researches on CPSCs and provide a systematic review of various types of regulation tools. As a multipart device, the properties of each part of CPSCs have their own impact on the overall device performance and are different from those of PSCs with conventional metal electrodes. Therefore, in combining the unique structural features of CPSCs, we review research progress on the following aspects of CPSCs: modulation of electron transport layers (ETLs) and HTLs, interfacial modulation, modulation of perovskite layers, and modulation of carbon-electrode materials. This review aims to systematically identify the optimization strategies for each part of CPSC devices and to promote new work to enhance the PCE of CPSCs and make them more advantageous for large-scale commercial manufacturing.

2. Transporting layer design

The charge transporting layer is a vital component of CPSCs with n-i-p architecture, and the performance of the ETL/hole blocking layer (HBL) and HTL/electron blocking layer (EBL) determines the efficiency of selective charge extraction and transport (tables 1 and 2).

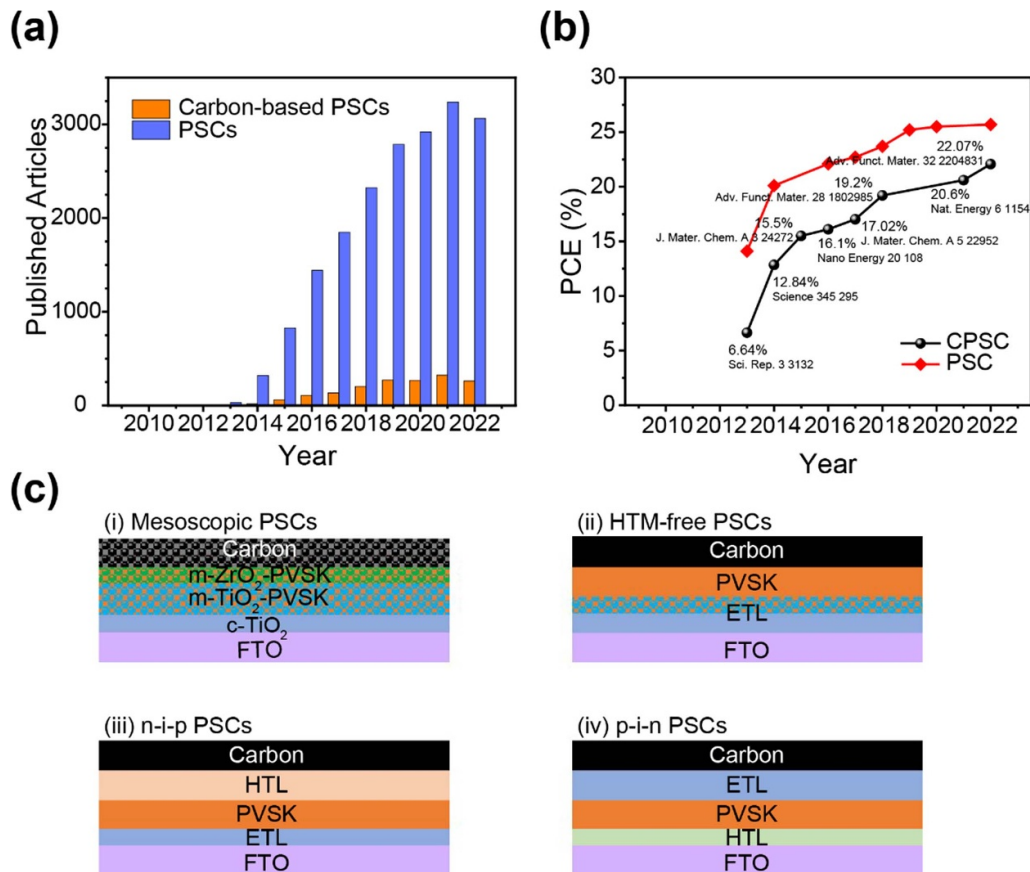


Figure 1. (a) Published article statistics from Web of Science. (b) Reported PCE evolution of PSCs and CPSCs. (c) Four main architectures during the development of CPSCs: mesoscopic (i), HTL-free (ii), n-i-p (iii), and p-i-n (iv) PSCs.

2.1. ETL/HBL for CPSCs

In the CPSCs of the n-i-p architecture, due to excellent energy-level alignment and electron mobility, TiO₂ and SnO₂ are often considered as the suitable ETLs [9, 16–19]. Many researchers focused on optimizing the performance of the ETL to improve charge separation and transport to enhance the relatively low PCE of CPSCs. Liu *et al* first demonstrated CPSCs using Ni-doped rutile TiO₂ as ETL [20]. They found that Ni doping can shift up the Fermi level of the ETL and increase the charge mobility of the TiO₂, therefore enhancing the charge transport and extraction. Ultraviolet photoelectron spectroscopy (UPS), displayed in figure 2(a), reveals the impact of Ni doping on the TiO₂ electronic structure. The distances between the valence band (VB) and the Fermi level are about 3.40 eV and 3.38 eV for the pristine TiO₂ and Ni:TiO₂, respectively. The upward shift of the Fermi level promotes extraction of the charge. As a result, they achieved a high PCE of 17.46% for the CPSCs. Liu *et al* reported a low-temperature (70 °C) solution-processed Mg-doped rutile TiO₂ as ETL in CPSCs (figure 2(b)) [21]. The efficient charge extraction, better electrical conductivity, and suppressed charge recombination of Mg-doped TiO₂ resulted in a higher PCE of 15.73% compared to the PCE of pristine TiO₂-based device.

However, the results of studies conducted by several authors have shown that SnO₂ could be a better candidate

for ETL because of its high mobility, good stability, and low photoactivity [22–24]. Replacing TiO₂ with SnO₂ helps to improve the PCE of CPSCs. Besides, several reports have demonstrated that rational doping of SnO₂ can improve the performance of CPSCs. Ye *et al* first reported low-temperature, processed, Zn-doped SnO₂ as an effective ETL in CPSCs with CuPc HTL [25]. They found that Zn doping contributes to a more suitable energy-level alignment (figure 2(f)) and an improved conductivity of SnO₂ films. More importantly, Zn doping elevated the Fermi level of the ETL, contributing to a more powerful built-in electric field in the device and a wider depletion region. For this reason, the electron transfer and extraction are improved, and the charge recombination is suppressed. Finally, CPSCs with Zn:SnO₂ ETL achieve a champion PCE of 17.78%, V_{OC} of 1.098 V, short-circuit current density J_{SC} of 23.4 mA cm⁻², and fill factor (FF) of 0.692. It is worth noting that the PCEs of CPSCs using SnO₂ ETL are mostly higher than TiO₂-based CPSCs; thus, there is a trend to gradually replace TiO₂ by SnO₂ in CPSCs. Besides, Khambunkoed *et al* achieved fully covered and compact ZnO ETL via a homemade slot-die coater setup on a three-axis CNC platform. With the optimized ZnO ETL, CPSCs offered the highest PCE of 10.81% [26].

Another effective way to build a high-performance ETL is to use a two-layer structure. In the all-inorganic system, Liu *et al* achieved the highest PCE for CsPbBr₃ CPSCs by

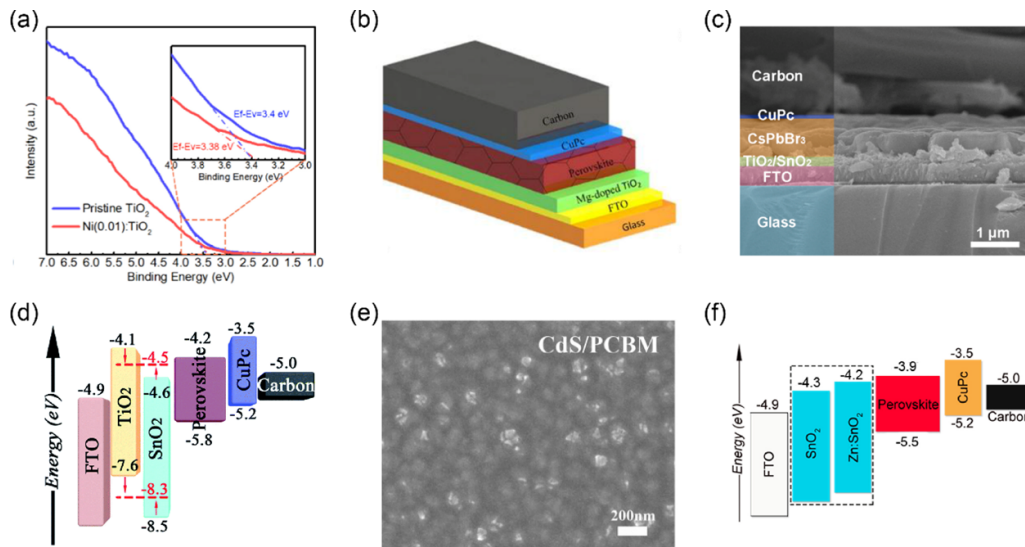


Figure 2. (a) UPS of Ni-doped TiO₂ ETL [20]. Reprinted from [20], Copyright (2018), with permission from Elsevier. (b) Mg-doped rutile TiO₂ as ETL in CPSCs [21]. Reprinted from [21], Copyright (2018), with permission from Elsevier. (c) SEM image of the device with TiO₂/SnO₂ ETL [27]. Reprinted from [27], Copyright (2019), with permission from Elsevier. (d) The energy-level arrangement of CPSCs with TiO₂/SnO₂ bilayer [28]. Reproduced from [28] with permission from the Royal Society of Chemistry. (e) SEM image of the PCBM-coated CdS [29]. Reprinted from [29], Copyright (2019), with permission from Elsevier. (f) Energy-level alignment of CPSCs with Zn-doped SnO₂ ETL [25]. Reprinted from [25], Copyright (2019), with permission from Elsevier.

Table 1. Summary of performance parameters of CPSCs with different types of ETLs.

ETL	Device structure	V _{OC} (V)	J _{SC} (mA cm ⁻²)	FF	PCE (%)	References
Ni:TiO ₂	FTO/TiO ₂ /Cs-MA-FA/CuPc/carbon	1.07	22.41	0.73	17.46	[20]
Mg:TiO ₂	FTO/TiO ₂ /Cs-MA-FA/CuPc/carbon	1.03	22.26	0.69	15.73	[21]
Zn: SnO ₂	FTO/Zn: SnO ₂ /Cs-MA-FA/CuPc/carbon	1.10	23.40	0.69	17.78	[25]
ZnO	FTO/ZnO/Cs-FA/spiro-OMeTAD/carbon	0.96	15.53	0.73	10.81	[26]
TiO ₂ /SnO ₂	FTO/TiO ₂ /SnO ₂ /CsPbBr ₃ /CuPc/carbon	1.31	8.24	0.81	8.79	[27]
TiO ₂ /SnO ₂	FTO/TiO ₂ /SnO ₂ /Cs-MA-FA/CuPc/carbon	0.98	23.28	0.67	15.39	[28]
CdS/PCBM	FTO/CdS/PCBM/Cs-MA-FA/CuPc/carbon	1.00	20.86	0.60	14.28	[29]

Cs-MA-FA: triple-cation perovskite; Cs-FA: double-cation perovskite.

applying SnO₂ to passivate the compact TiO₂ (c-TiO₂) ETL [27]. As shown in the scanning electron microscope (SEM) image in figure 2(c), the TiO₂/SnO₂ bilayered ETL possesses an excellent electron extraction capability and contributes to the charge transport and suppression of the interfacial trap-assisted recombination. The SnO₂ layer can not only improve the surface morphology of the ETL but also reduce the current shunting pathways in the c-TiO₂. They found fewer trap states in the CsPbBr₃ film deposited on the SnO₂-passivated TiO₂ film via photoluminescence (PL) spectroscopy measurements. As a result, the champion PCE of the as-prepared CsPbBr₃ CPSCs is promoted from 7.05% to 8.79%. Liu *et al* reported a TiO₂/SnO₂ bilayer as ETL for CPSCs, yielding a high PCE of 15.39% and excellent stability over 1200 h [28]. The TiO₂/SnO₂ bilayer is beneficial for electron transport, thus resulting in a suppressed charge recombination and appropriate energy-level arrangement (figure 2(d)). In addition, devices with TiO₂/SnO₂ bilayer had a wider depletion region in favor of enhanced photovoltaic performance. They found that after coating SnO₂, the conduction band (CB) of ETL was adjusted from -4.2 eV to -4.5 eV. A deep CB of ETL means a

strengthening of the Fermi-level splitting, which leads to a high V_{OC}. Liu *et al* first introduced CdS ETL into CPSCs and decorated the CdS/perovskite interface with PCBM [29]. An SEM image of the PCBM-coated CdS is given in figure 2(e). The PCBM layer is capable of covering the CdS film and filling the cracks between every CdS nanoparticle. Through the steady-state PL characterization, the quenching efficiencies of CdS and CdS/PCBM are calculated as 79% and 94%, respectively. This result demonstrated that the CdS/PCBM composite ETL promotes the transfer of charge and effectively suppresses the recombination of charge. Therefore, PCBM decoration can promote the separation and hinder the recombination of charge. The PCE of the optimal CdS/PCBM device was further improved to 14.28% compared with 13.22% of the CdS-based device.

2.2. HTL/EBL for CPSCs

To date, most CPSCs, especially the all-inorganic CPSCs, have HTL-free structures. The interfacial energy barrier at the perovskite/carbon interface induces undesirable charge

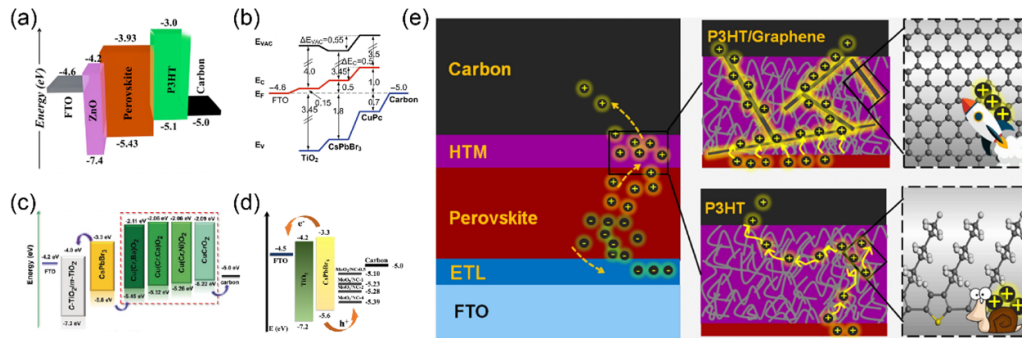


Figure 3. (a) Energy-level alignment of P3HT-based CPSCs [31]. Reprinted from [31], Copyright (2021), with permission from Elsevier. (b) Schematic energy-level alignment at interfaces. E_{VAC} is the vacuum energy, E_C is the CB edge, E_F is the Fermi level, and E_V is the VB edge [33]. Reproduced from [33]. CC BY 4.0. (c) The energy-level distribution of the PSCs with Cu(Cr, M) O_2 HTL. [36] John Wiley & Sons. [© 2019 Wiley-VCH Verlag GmbH & Co. KGaA, Weinheim]. (d) Energy-level diagram of all-inorganic CsPbBr $_3$ CPSCs with MoO $_2$ /NC-x HTL [40]. Reprinted from [40], Copyright (2020), with permission from Elsevier. (e) Illustration of CPSCs with P3HT HTL and P3HT/graphene composited HTL, respectively [38]. Reprinted from [38], Copyright (2019), with permission from Elsevier.

Table 2. Summary of performance parameters of CPSCs with different types of HTLs.

HTL	Device structure	V_{oc} (V)	J_{sc} (mA cm $^{-2}$)	FF	PCE (%)	References
P3HT	FTO/ZnO/CH $_3$ NH $_3$ PbI $_3$ /P3HT/carbon	1.02	20.62	0.76	16.05	[31]
P3HT	FTO/Nb $_2$ O $_5$ /Cs $_3$ Sb $_2$ I $_{9-x}$ Cl $_x$ /P3HT/carbon	0.80	3.87	0.53	1.67	[32]
CuPc	FTO/TiO $_2$ /CsPbBr $_3$ /CuPc/carbon	1.26	6.62	0.74	6.21	[33]
CuPc	FTO/TiO $_2$ /CH $_3$ NH $_3$ PbI $_3$ /CuPc/carbon	1.05	20.8	0.74	16.1	[10]
CuInS $_2$ /ZnS QDs	FTO/c-TiO $_2$ /m-TiO $_2$ /CsPbBr $_3$ /CuInS $_2$ /ZnS QDs/carbon	1.62	7.73	0.86	10.85	[35]
Cu(Cr,M)O $_2$	FTO/c-TiO $_2$ /m-TiO $_2$ /CsPbBr $_3$ /Cu(Cr,M)O $_2$ /carbon	1.62	7.81	0.86	10.79	[36]
P3HT/Ta-WO $_x$	ITO/SnO $_2$ /MAPbI $_3$ /P3HT/Ta-WO $_x$ /carbon	1.12	22.5	0.72	18.1	[37]
P3HT/graphene	FTO/SnO $_2$ at TiO $_2$ /FA $_{0.3}$ MA $_{0.7}$ PbI $_3$ /P3HT/graphene/carbon	1.09	22.5	0.74	18.2	[38]
P3HT/ZnPc	FTO/TiO $_2$ /CsPbBr $_3$ /P3HT/ZnPc/carbon	1.58	7.65	0.83	10.03	[39]
MoO $_2$ /NC	FTO/c-TiO $_2$ /m-TiO $_2$ /CsPbBr $_3$ /MoO $_2$ /NC/carbon	1.53	7.20	0.85	9.40	[40]
CuSCN/Ta-WO $_x$	ITO/SAM/MAPbI $_3$ /CuSCN/Ta-WO $_x$ /carbon	1.01	17.21	0.71	12.31	[41]

accumulation and recombination, which results in a lower PCE compared to PSCs with metal electrodes. The appropriate HTL could efficiently improve hole extraction to carbon electrodes [30].

Most of the HTLs commonly used in CPSCs are organic materials, such as poly(3-hexylthiophene-2,5-diyl) (P3HT) and CuPc, for low-cost solution processing and commercial production. Jin *et al* reported a typical p-type P3HT as HTL for CPSCs with ZnO ETL, and the energy-level alignment of P3HT-based PSCs is shown in figure 3(a) [31]. The highest occupied molecular orbital (HOMO) and the lowest unoccupied molecular orbital (LUMO) levels of P3HT are -5.1 eV and -3.0 eV, respectively. The LUMO level of P3HT is higher than the CB of CH $_3$ NH $_3$ PbI $_3$ (-3.93 eV), and the HOMO level is lower than the Fermi level of carbon (-5.0 eV) and higher than the VB of CH $_3$ NH $_3$ PbI $_3$ (-5.43 eV). The appropriate arrangement of energy levels could block the electron in perovskite and promote the hole extraction to carbon. Therefore, the appropriate P3HT HTL suppressed the carrier recombination and achieved PCE as high as 16.05%. Zhao *et al* reported a novel strategy that uses P3HT as HTL for lead-free CPSCs [32]. They found that P3HT has a suitable energy level and high hole-transport rate with low carrier non-radiative recombination. As a result, the Cs $_3$ Sb $_2$ I $_{9-x}$ Cl $_x$ solar cell achieved a higher PCE of 1.67%. Liu *et al* applied CuPc as HTL for

CPSCs (figure 3(b)) [33]. The CB offset between the CsPbBr $_3$ layer and the CuPc layer provides an energy barrier that prevents electrons from flowing to the CuPc layer, whereas the VB offset provides an additional driving force for the flow of holes to the CuPc layer. Moreover, depositing thin CuPc can also passivate defects on the surface of CsPbBr $_3$ as well as induce a large interfacial area of CuPc, correspondingly favoring the hole transported from CuPc to carbon. Finally, the optimal device acquired a decent PCE of 6.21%, over 60% higher than those of the HTL-free devices. Zhang *et al* applied CuPc nanorods as HTL for printable low-temperature processed CPSCs [10]. The strong π - π stacking between layered CuPc molecules favors the formation of high carrier mobility [34]. In addition, depositing thin CuPc contributes to a good contact with counter electrode, which favors the hole transported from CuPc to carbon. They achieved an impressive PCE of 16.1%, which is the highest PCE for the CPSCs at that time.

In addition, quantum dots and inorganic materials can also be used as efficient HTL. Duan *et al* demonstrated alkyl-chain-regulated quantum dots as HTL to suppress charge recombination [35]. They precisely controlled alkyl-chain length of ligands to maximize charge extraction by balancing the surface dipole-induced charge coulomb repulsive force and quantum tunneling distance. Finally, the inorganic CsPbBr $_3$ CPSC achieves a champion PCE up to 10.85%. Duan *et al*

reported p-type $\text{Cu}(\text{Cr}, \text{M})\text{O}_2$ (where $\text{M} = \text{Ba}^{2+}$, Ca^{2+} , or Ni^{2+}) nanocrystals with improved hole-transport properties by increasing interstitial oxygen to effectively extract holes from perovskite [36]. The larger ions induced lattice expansion allows more interstitial oxygen atoms to be inserted into the host CuCrO_2 lattice, contributing to improved hole conductivity. Therefore, inorganic $\text{Cu}(\text{Cr}, \text{M})\text{O}_2$ HTL conduces to enhancing hole extraction from perovskite and reducing carrier recombination. Besides, the energy-level distribution is compatible with that of CsPbBr_3 perovskite layer and carbon electrode, as shown in figure 3(c). The optimized CsPbBr_3 solar cell with $\text{Cu}(\text{Cr}, \text{Ba})\text{O}_2$ HTL achieves a champion PCE as high as 10.79%.

Constructing a double-layer HTL is also an effective method to improve the PCE of CPSCs. Yang *et al* reported that the PCE of CPSCs was increased up to 18.1% by employing a double layer of P3HT/ tantalum-doped tungsten oxide (Ta-WO_x) as the HTL [37]. They prepared P3HT/ Ta-WO_x using a blade-coating process, which solves the problem of the shallow HOMO level of P3HT resulting in a lower V_{OC} and strong electronic coupling between the flat P3HT molecules and perovskites. By incorporating P3HT into CPSCs, the V_{OC} of CPSCs was greatly improved to 1.12 V. Chu *et al* developed a low-temperature solution-processed P3HT/graphene composite HTL, which exhibits outstanding charge mobility and thermal tolerance, with high hole mobility, as shown in figure 3(e) [38]. By SEM, HTL films appear homogeneous, indicating that the graphene is beneficial for promoting hole transport to the carbon electrode. The PL decay of the P3HT/graphene samples (43 ns) is slightly faster than the pure P3HT samples (55 ns), indicating improved hole extraction at the perovskite/HTL interface. As a result, the P3HT/graphene composite HTL device yielded an enhanced PCE of 18.2% compared to the pure P3HT device with a PCE of 11.1%. Liu *et al* reported a P3HT/zinc phthalocyanine (ZnPc) composite with a tunable energy level, which was employed as the HTL in CsPbBr_3 CPSCs [39]. P3HT/ZnPc HTL is in favor of reducing the energy-level difference and passivating the surface defects of perovskite, promoting charge separation and reducing charge recombination at CsPbBr_3 /carbon interface. As a result, the authors achieved a champion PCE of 10.03%, which suggests that P3HT/ZnPc composite is an efficient HTL for high-efficiency CsPbBr_3 CPSCs. Zong *et al* reported an MoO_2 /N-doped carbon nanosphere (NC) composite with high hole mobility and matched energy level, which is prepared by a facile one-step pyrolysis process and introduced into all-inorganic CsPbBr_3 CPSCs as the HTL [40]. The MoO_2 /NC HTL not only enhances energy-level alignment, interface contact, and charge extraction, but it also passivates CsPbBr_3 surface defects, thus leading to the reduction of energy loss and charge recombination. As shown in figure 3(d), all the work functions (WFs) of MoO_2 /NC-x composites are between the VB of CsPbBr_3 and the WF of carbon electrode, indicating that the introduction of MoO_2 /NC composited HTL can reduce the interface energy offset and therefore energy loss. Finally, the authors achieved a maximum PCE of 9.40%, which is much higher than those of HTL-free devices. Mashhoun *et al* achieved a PCE of 12.31% for

CPSCs utilizing doped CuSCN as HTL [41]. They coated the nanoparticulate Ta-WO_x layer on top of CuSCN , contributing to well-matched energy levels between the VBs of CuSCN and $\text{CH}_3\text{NH}_3\text{PbI}_3$ and the high hole mobility, as well as improving the hole extraction property of HTL. As a result, the PCE was improved from 8.59% to 12.31%. In addition, the Ta-WO_x layer can protect the HTL interface from the negative impact of the carbon ink's solvent.

In conclusion, the HTLs employed in CPSCs are mainly p-type wide-bandgap semiconductors. From previous reports, P3HT and CuPc are the most commonly used HTLs with good stability, high conductivity, and energy-level matching.

3. Interface engineering for perovskite active layer

The interfaces (buried and upper interfaces) in CPSCs of the n-i-p architecture largely influence the charge transfer and recombination behavior. In general, carbon electrodes obtained from common commercial carbon paste do not have the same transport capability as metal electrodes. In addition, due to the special semiconductor nature of all-inorganic perovskite, the photogenerated carrier separation generally occurs in the interface of ETL and the perovskite layer, which, together with the certain hole-transport capability of carbon electrodes, makes all-inorganic CPSCs usually omit the HTL. As a result, the ETL/perovskite interface of the CPSC suffers from severe carrier non-radiative recombination, and the charge separation and transfer are hindered. In the case of organic-inorganic hybrid perovskite, charge extraction and transport at both the upper and buried interfaces are critical; otherwise, it will lead to carrier transport imbalance, and thus carrier accumulation and quenching at the interface. In addition, the introduction of interfacial modification layers not only helps to enhance carrier transport, reduce non-radiative recombination, and improve the overall device performance, but it also helps to attenuate ion migration and damage to the lower layer caused by carbon paste or HTL.

Several researchers have applied different types of materials, such as organic salts [42], inorganic compounds [43–47], metal oxides [48], ionic liquids [49], fullerenes [14, 50], self-assembled monolayers (SAMs) [51], and organic polymers [52], to improve the quality of the buried interface, thereby improving the quality of the perovskite film crystallinity; passivating interfacial defects; regulating the interfacial energy band alignment; and enhancing interfacial contacts to suppress the occurrence of non-radiative recombination and accelerate interfacial charge extraction and transfer through interfacial engineering (table 3).

Zhu *et al* modified the TiO_2 as well as perovskite films simultaneously by introducing ammonium chloride (NH_4Cl) into the interface, which not only improved the contact and energy-level matching at the TiO_2 /perovskite interface but also provided high-quality perovskite films with larger grain size by modulating the crystallization kinetics of CsPbBr_3 through ion binding and passivation, resulting in a significant enhancement of charge extraction and achieving up to 10.12% of PCE. In addition, the optimized device, without any encapsulation,

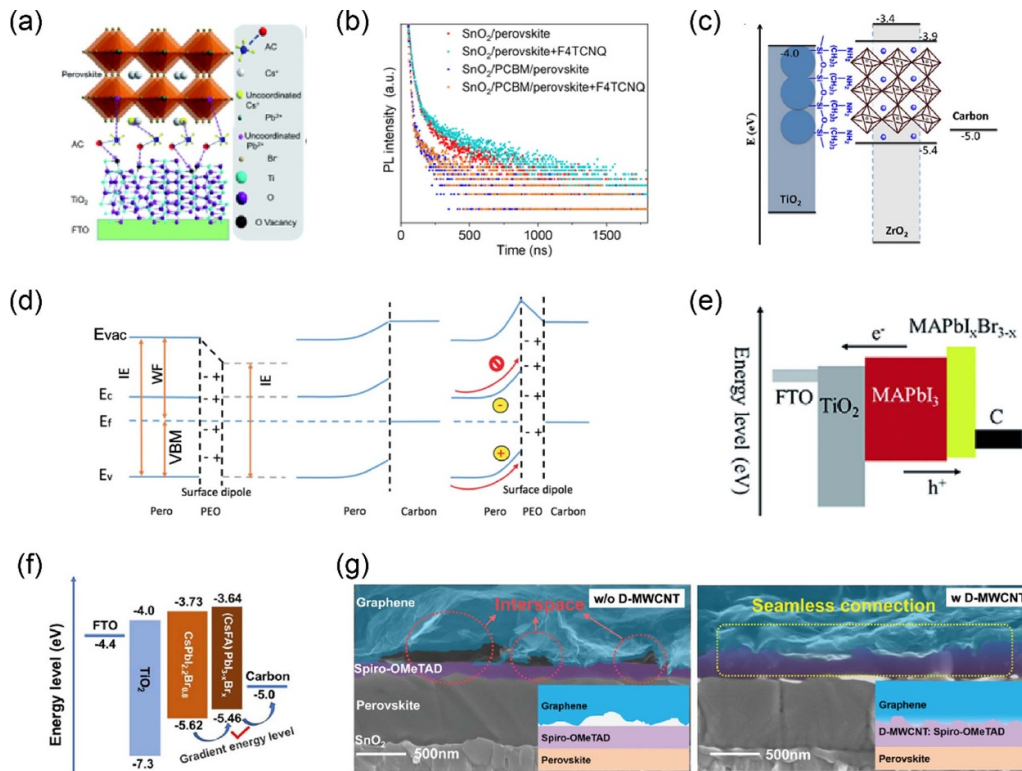


Figure 4. (a) Schematic diagram about the function of NH₄Cl at the TiO₂/perovskite interface [47]. Reproduced from [47] with permission from the Royal Society of Chemistry. (b) Time-resolved photoluminescence spectra of the perovskite deposited on the different ETLs [14]. Reprinted from [14], with the permission of AIP Publishing. (c) Energy band diagram of the device and the organic silane SAM between the TiO₂ surface and the perovskite [51]. Reprinted with permission from [51]. Copyright (2015) American Chemical Society. (d) Schematic illustration of the energy-level diagram of the interface. Note that here the ionization energy value for the PEO-modified perovskite sample is obtained for the perovskite film mixed with PEO. [57] John Wiley & Sons. [© 2019 The Authors. Published by WILEY-VCH Verlag GmbH & Co. KGaA, Weinheim]. (e) Energy-level diagram of each material in the PSC [60]. Reproduced from [60] with permission from the Royal Society of Chemistry. (f) Energy-level diagram of FTO/TiO₂/CsPbI_{2.2}Br_{0.8}/(CsFA)PbI_{3-x}Br_x/carbon. [64] John Wiley & Sons. [© 2021 Wiley-VCH GmbH]. (g) False-colored cross-sectional SEM images of CPSCs using Spiro-OMeTAD HTLs without and with D-MWCNT modification. Insets more visibly illustrate their different contact conditions at the HTL/graphene interface. [12] © 2022 Wiley-VCH GmbH].

exhibited a long-term stability of 720 h at 25 °C and 80% relative humidity (RH) in air environment (figure 4(a)) [47]. Zou *et al* introduced a PCBM-modified layer on the SnO₂ layer, and the bottom interface modification made the perovskite films obtained based on this interface show a uniform and compact morphology with large grains without any pinholes or PbI₂ impurities on the grain boundaries, while the PCBM also served to passivate the interfacial defects and accelerate charge extraction and transfer, suppressing the carrier non-radiative recombination at the ETL/perovskite interface and obtaining 15.1% of PCE (figure 4(b)) [14]. Liu *et al* inserted an organic silane SAM between TiO₂ and perovskite layers, which helped to tune the electronic structure of the interface and passivate the defects, resulting in optimized interfacial energy-level alignment and carrier lifetime growth, and the PCE of TiO₂/SAM/CH₃NH₃PbI₃-based mesoscopic solar cells was as high as 12.7% (figure 4(c)) [51]. Yuan *et al* addressed the energy-level difference and severe charge recombination of TiO₂/CsPbBr₃ interface by modifying the interface with carbon quantum dots (CQDs). By setting the intermediate energy levels, electron extraction is significantly enhanced, and the optimized PSC achieves a PCE of 7.93%.

In addition, the long-term stability of the unencapsulated PSCs exceeded 1400 h at 80% RH [53].

Similar to the buried interface, the main problems to be solved for the upper interfaces of CPSCs are poor contact due to the rough surface of the perovskite and carbon electrodes, poor hole extraction and transport ability, severe surface defects resulting in non-radiative recombination at the interface, and energy-level mismatch between the layers. As a result, researchers have used organic polymers [54–57], organic salts [58–66], inorganic materials [67, 68], and carbon nanotubes [12, 69, 70] for interface engineering to improve the quality of the interface, enhance the film crystallinity quality of perovskite, passivate interfacial defects, improve the interfacial energy band alignment, enhance the interfacial contact, build a hole transfer channel and act as an EBL to reduce the carrier non-radiative recombination, and accelerate the hole extraction and transfer at the interface.

By introducing a functional polymethyl methacrylate (PMMA) layer on the surface of the all-inorganic lead-free Cs₂AgBiBr₆ double perovskite, Li *et al* avoided direct contact between the carbon and the underlying charge-transfer layer and passivated the surface defects, inhibiting

Table 3. Summary of performance parameters of CPSCs with different types of interface of engineering.

Interface material	Structure of device	J_{sc}				References
		V_{OC} (V)	(mA cm^{-2})	FF	PCE (%)	
NH ₄ Cl	FTO/c-TiO ₂ /m-TiO ₂ /NH ₄ Cl/CsPbBr ₃ /carbon	1.61	7.64	0.82	10.12	[47]
PCBM	FTO/SnO ₂ /PCBM/Cs _{0.09} FA _{0.27} MA _{0.64} PbI ₃ + F4TCNQ/P3HT/carbon	1.07	22.23	0.64	15.10	[14]
SAM	FTO/c-TiO ₂ /m-TiO ₂ /SAM/MAPbI ₃ /ZrO ₂ /carbon	0.87	19.51	0.75	12.77	[51]
CQD	FTO/c-TiO ₂ /m-TiO ₂ /CQDs/CsPbBr ₃ /PQDs/carbon	1.45	7.24	0.76	7.93	[53]
PMMA	FTO/c-TiO ₂ /m-TiO ₂ /Cs ₂ AgBiBr ₆ /PMMA/carbon	1.18	2.82	0.68	2.25	[55]
PVAc/GO	FTO/c-TiO ₂ /m-TiO ₂ /CsPbBr ₃ /PVAc/GO/carbon	1.55	7.41	0.83	9.53	[56]
PEO	FTO/c-TiO ₂ /m-TiO ₂ /FA _{0.8} Cs _{0.2} PbI _{2.64} Br _{0.36} /PEO/carbon	1.08	21.20	0.65	14.90	[57]
MABr	FTO/c-TiO ₂ /m-TiO ₂ /MAPbI ₃ /MAPbI _x Br _{3-x} /carbon	1.07	20.80	0.73	16.20	[60]
PEAI	FTO/c-TiO ₂ /m-TiO ₂ /MA _{0.16} FA _{0.79} Cs _{0.05} Pb(I _{0.84} Br _{0.16}) ₃ /PEA ₂ PbI ₄ /carbon	1.07	21.44	0.68	15.66	[62]
OAI	FTO/c-TiO ₂ /m-TiO ₂ /FAPbI ₃ /(OA) ₂ PbI ₄ /carbon	1.03	24.30	0.74	18.50	[63]
FAI	FTO/c-TiO ₂ /CsPbI ₂ Br/(CsFA)PbI _{3-x} Br _x /carbon	1.18	15.72	0.81	15.03	[64]
CsCl	FTO/c-TiO ₂ /m-TiO ₂ /CsPbI ₃ /Cs ₂ PbI ₂ Cl ₂ /carbon	1.21	18.30	0.74	15.23	[67]
Cs ₂ PtI ₆	ITO/SnO ₂ /SnCl ₂ /CsPbI ₂ Br/Cs ₂ PtI ₆ /carbon	1.28	14.85	0.72	13.69	[68]
D-MWCNT	FTO/SnO ₂ /FA _x MA _{1-x} PbI ₃ /D-MWCNT: Spiro-OMeTAD/graphene/FTO	1.08	25.97	0.79	22.07	[12]

the non-radiative carrier recombination from poor film quality and accelerating the interfacial charge extraction. In addition, the unencapsulated devices maintain nearly 100% of their initial PCE after 80 d of storage at 25 °C and 5% RH or 60 d of storage at 85 °C and 0% RH due to the PMMA layer's resistance to corrosion by water and oxygen [55]. Ding *et al* inserted a carbonyl-modified polyvinyl acetate (PVAc) polymer as an interfacial modification at the CsPbBr₃/carbon interface, which passivated the surface defects of perovskite and improved the energy-level alignment between the VB of CsPbBr₃ and the WF of carbon, inhibiting carrier recombination and accelerating charge separation. A graphene oxide (GO) layer is also introduced to further promote hole extraction and reduce the energy-level mismatch. The FTO/c-TiO₂/m-TiO₂/CsPbBr₃/PVAc/GO/Carbon-based PSC achieved a champion PCE of up to 9.53%, with a 44.0% improvement compared to the control device, and significant long-term stability under high humidity, high temperature, and continuous illumination in air environment [56]. Wu *et al* introduced a thin layer of poly(ethylene oxide) (PEO) to modify the perovskite/carbon interface to achieve an improved interfacial energy-level alignment for efficient charge transfer, and they obtained an increase in PCE from 12.2% to 14.9% with good stability under double-85 aging conditions without encapsulation (figure 4(d)) [57].

Liu *et al* used MABr to *in situ* grow a methylammonium lead mixed halide (MAPbI_xBr_{3-x}) perovskite layer on the top of an MAPbI₃ perovskite layer to form an MAPbI₃/MAPbI_xBr_{3-x} perovskite stacking structure, which formed a favorable interfacial energy-level alignment and reduced the carrier recombination at the perovskite/carbon-electrode interface. An optimized device with a PCE of 16.2% was obtained, and good storage stability was also exhibited under continuous light and dark conditions (figure 4(e)) [60].

Lee *et al* post-treated a carbon electrode with phenylethylammonium iodide (PEAI) to grow an ultrathin 2D perovskite PEA₂PbI₄ layer at the interface between the 3D perovskite and carbon layers, which improved the poor perovskite/carbon contact and greatly inhibited the interfacial charge

recombination, increasing the average PCE of the device from 11.5% to 14.5%, reducing the hysteresis loss, achieving a maximum PCE of 15.6%, and showing good environmental stability and thermal stability [62]. Similarly, Zouhair *et al* introduced a 2D perovskite passivation layer (OA)₂PbI₄ as an EBL at the perovskite/carbon interface to significantly reduce the interfacial recombination loss, thereby increasing the FF and V_{OC} , obtaining a high efficiency of 18.5%, and greatly improving device stability [63]. Wang *et al* constructed an *in situ* perovskite transition layer (CsFA)PbI_{3-x}Br_x film with an intermediate energy level between CsPbI_{2.2}Br_{0.8} and carbon electrode by ion exchange through a simple formamidinium iodide (FAI) post-treatment strategy to extend the light absorption edge of CsPbI_{2.2}Br_{0.8} from 657 nm to 680 nm. In addition, the transition layer can also serve as a hole transfer channel between CsPbI_{2.2}Br_{0.8} and the carbon electrode due to its suitable intermediate energy level and effective defect passivation. As a result, the optimized CPSC achieves a champion PCE of 15.03% and an ultrahigh FF of 0.81, and the stability of the device is also improved (figure 4(f)) [64].

Wang *et al* used CsCl for surface treatment, and the CsCl residue tended to react with CsPbI₃ to generate 2D Cs₂PbI₂Cl₂ nanosheets as an EBL. The synergistic effect of the suitable energy-level gradient and the EBL well improved the hole selectivity at the CsPbI₃/carbon interface to reduce the carrier recombination loss, achieving an efficiency of 15.23% [67]. Similarly, Han *et al* used a 2D perovskite Cs₂PtI₆ to modify the surface of CsPbI₂Br to adjust the energy-level matching and suppress carrier recombination, and the excellent hydrophobic property of Cs₂PtI₆ retarded the degradation of the perovskite, and the optimized devices obtained higher PCE (13.69%) and stability [68].

Wang *et al* used defective multi-walled carbon nanotube (D-MWCNT) to tune the charge transfer kinetics at the interface between the HTL and the carbon electrodes. Electrostatic dipole moment interaction between the terminal oxygen-containing group of D-MWCNT and the Spiro-OMeTAD allowed the establishment of interfacial coupling at the molecular level through edge

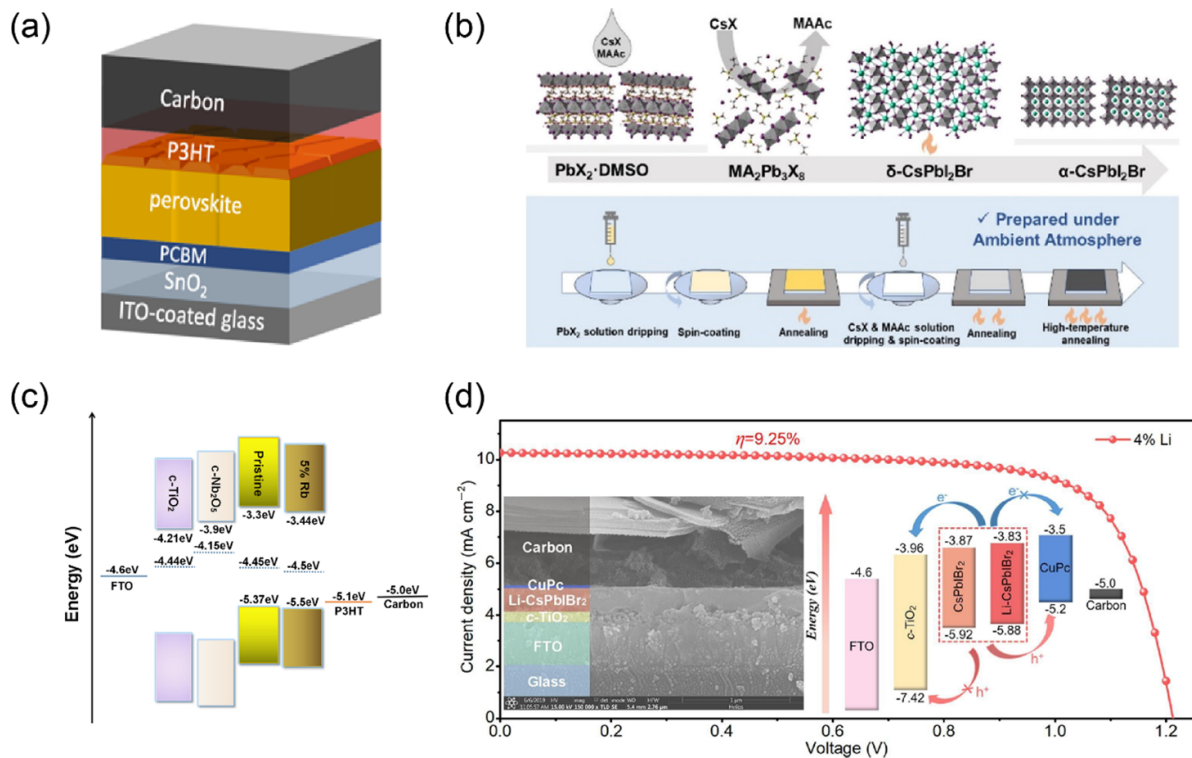


Figure 5. (a) Structure of optimized CPSC devices with F4TCNQ [14]. Reprinted from [14], with the permission of AIP Publishing. (b) Schematic illustration of the MAAc additive strategy with perovskite crystallization processes for the preparation of CsPbI₂Br inorganic perovskite films through two-step deposition [84]. Reprinted with permission from [84]. Copyright (2021) American Chemical Society. (c) Energy-level diagram of device with Cs₃Sb₂Cl_xI_{9-x}/Rb_{0.15}Cs_{2.85}Sb₂Cl_xI_{9-x} as absorber layer and TiO₂/Nb₂O₅ as ETL [89]. Reprinted from [89], Copyright (2021), with permission from Elsevier. (d) High-resolution cross-sectional SEM images of the whole devices with a configuration of FTO/c-TiO₂/Li-CsPbI₂Br₂/CuPc/carbon and device energy-level diagram [90]. Reprinted from [90], Copyright (2020), with permission from Elsevier.

effect-induced electron redistribution and 1D hyper-channels to achieve fast charge transfer. Meanwhile, the seamless connection between the HTL and the carbon electrodes was promoted due to the induced interfacial coupling between D-MWCNT and graphene at the nanometer scale. Based on this strategy, a high PCE of 22.07% (certified PCE of 21.9%) and excellent operational stability were achieved (figure 4(g)) [12].

4. Design of perovskite active layer

Towards the optimization of the perovskite layer in CPSCs, we need to take the special structure and properties of the CPSCs into account, in addition to the similar approach to obtain high-quality films for PCE enhancement as in metal PSCs. In systems where the carrier transport capability of the electrode and transporting layer has drawbacks, we need to work on obtaining high-quality thin films of the perovskite layer to obtain good interfacial contact, long carrier lifetime, and strong carrier transport capability. In addition to the incompatibility caused by the mutual destruction of the conventional HTL Spiro-OMeTAD and commercial carbon pastes [71], the instability of the devices caused by the commonly used HTL dopants, and the lack of transport capability of undoped HTL, it is necessary for us to precisely tune the energy band

structure of the perovskite surface to obtain a suitable energy-level match for CPSCs, combining with the development of new efficient transport materials. CPSCs are very promising for future commercialization due to their low cost and simple fabrication process, which requires us to explore production processes that can be manufactured in air environment on a large scale, at low cost, and with low energy consumption.

Therefore, researchers usually use composition engineering [72–74], solvent engineering [75–78], additive engineering [14, 79–82], intermediate-phase engineering [50, 83, 84], and optimization of film deposition methods [27, 85–88] to obtain high-quality perovskite films (table 4).

Zou *et al* used 2,3,5,6-tetrafluoro-7,7,8,8-tetracyanodi methane (F4TCNQ) as an additive in the perovskite precursor solution, which not only acts as passivation of defects and assists in crystallization of the film, but it also modulates to obtain more favorable interfacial energy band bending and energy-level matching while forming charge transfer complexes with perovskite due to its strong electron-withdrawing ability. Having all these features simultaneously allows the CPSCs added with F4TCNQ to obtain high-quality low-defect-density films with suppressed non-radiative recombination within the layers and at the interfaces, as well as extremely fast carrier separation and extraction capabilities, and the optimized CPSCs obtain an enhanced PCE of 15.1% and high V_{OC} of 1.07 V with long-term

Table 4. Summary of performance parameters of CPSCs with different fabrication methods of perovskite.

Method	Structure of device	J_{sc}				References
		V_{OC} (V)	(mA cm^{-2})	FF	PCE (%)	
Additive engineering	FTO/SnO ₂ /PCBM/Cs _{0.09} FA _{0.27} MA _{0.64} PbI ₃ + F4TCNQ/P3HT/carbon	1.07	22.23	0.64	15.10	[14]
Additive engineering	FTO/c-TiO ₂ /CsPbI ₂ Br + PVP/HTL/carbon	1.01	18.47	0.56	10.47	[82]
Intermediate-phase engineering	ITO/SnO ₂ /CsPbI ₂ Br (MAAc, EG)/carbon	1.27	14.2	0.62	11.2	[84]
Composition engineering	FTO/Nb ₂ O ₅ /Rb _{0.15} Cs _{2.85} Sb ₂ Cl _x I _{9-x} /P3HT/C	0.88	4.91	0.57	2.46	[89]
Composition engineering	FTO/c-TiO ₂ /Li-CsPbI ₂ Br ₂ /CuPc/carbon	1.22	10.27	0.74	9.25	[90]
Deposition method	FTO/c-TiO ₂ /SnO ₂ /CsPbBr ₃ /CuPc/carbon	1.31	8.24	0.81	8.79	[27]
Deposition method	FTO/c-TiO ₂ /CsPbI ₂ Br ₂ /CuPc/carbon	1.29	10.40	0.65	8.76	[91]

stability (figure 5(a)) [14]. Using additive engineering, Ullah *et al* fabricated polyvinylpyrrolidone (PVP) polymer-coated CsPbI₂Br stable phases at low temperatures (120 °C) to reduce trap states in perovskite films, thereby accelerating charge carrier separation and inhibiting carrier recombination. The optimized devices achieved a champion PCE of 10.47% [82].

Li *et al* innovatively proposed a strategy for two-step sequential deposition of methylamine acetate (MAAc) additive for air made of high-quality CsPbI₂Br films. By introducing MAAc into the CsX precursor solution, PbX₂ in the films was first converted to the intermediate-phase MA₂Pb₃X₈, which could then be completely converted to δ -CsPbI₂Br. Ethylene glycol (EG) was added to the CsX precursor solution to improve the homogeneity of the CsPbI₂Br films. The carbon-based CsPbI₂Br planar PSCs fabricated under an ambient atmosphere of 15% RH can achieve a champion PCE of 11.2% and maintain an initial efficiency value of 79.3% after aging under 15% RH at room temperature for 360 h (figure 5(b)) [84].

Guo *et al* manipulated the crystallization and improved the film quality of Cs₃Sb₂Cl_xI_{9-x} by partially exchanging the A-site inorganic cation with Rb or K, inhibiting the 0D phase generation and reducing the pinholes in the film to obtain 2.46% PCE of CPSCs (figure 5(c)) [89]. Similarly, Tan *et al* obtained highly crystalline and well-oriented CsPbI₂Br crystals with higher film coverage on the substrate, larger grains, and fewer grain boundaries through Li doping. The trap state density in the CsPbI₂Br films was also effectively mitigated, leading to longer carrier lifetime and reduced energy losses. A PCE of 9.25% was achieved, along with excellent air and thermal stability (figure 5(d)) [90].

Liu *et al* developed a facile multistep spin-coating strategy to deposit CsPbBr₃ films with higher phase purity and larger average grain sizes (1 μm) by tuning the number of CsBr spin-coating cycles. The enhanced film crystallinity and light-harvesting ability, as well as the reduction of trap states, enabled the planar CsPbBr₃ CPSC to achieve a champion PCE of 8.79% with good humidity and thermal stability [27]. Liu *et al* developed a novel vapor-assisted deposition strategy. PbBr₂ thin films were fabricated by an anti-solvent-washing technique, followed by vacuum evaporation of CsI onto the PbBr₂ layer. By precisely tuning the thickness of the CsI films, highly phase-pure and crystallized CsPbI₂Br films

were successfully obtained, exhibiting uniform morphology and comprehensive coverage of the substrate with grain sizes as large as micrometer scale and ultrahigh light absorption capability. The corresponding CPSCs achieved a champion PCE of 8.76% and an excellent V_{OC} of 1.289 V. The unencapsulated devices exhibited good moisture and thermal stability [91].

5. Carbon-electrode exploration

Many carbon materials have been applied in electronics for decades since fullerene was first fabricated in 1985 [92]. Among these options, graphite and carbon black are two alternatives of electrodes in commercial solar cells for their excellent conductivity and low cost [7]. Because of the suitable WF of 5.0 eV, solution-processible property, and material stability of these electrodes, they possess compatibility for commercial large-scale PSC manufacturing.

Because the key efficiency and stability problems, as well as their solutions in CPSCs, have been discussed in the previous sections, only the modification and innovation of carbon electrodes are discussed here. As for the PSC applications with n-i-p architectures, carbon pastes should fit in the under HTL, including energy level and solution compatibility. In consideration of large-scale manufacturing and commercialization, low-temperature-process compatible carbon-electrode materials are preferred.

As for the n-i-p device architecture, with the commonly used Spiro-OMeTAD as HTL, the challenge is on how to avoid the destruction of Spiro-OMeTAD by the solvent of carbon pastes. Zhang *et al* developed a sort of self-adhesive macroporous carbon electrode by a room-temperature solvent-exchange method (figures 6(a) and (b)) [13]. They bladed carbon pastes on a glass substrate and then soaked it into ethanol to remove residual solvent. After drying, the carbon electrode was peeled off from the substrate and directly adhered to the surface of Spiro-OMeTAD. Finally, they got a PCE up to 19.2%, with J_{SC} of 23.33 mA cm^{-2} , V_{OC} of 1.08 V, and FF of 0.76. Because the commercial carbon pastes commonly contain detrimental solvents, such as chlorobenzene and xylene, replacement of HTL is necessary, as discussed previously. Recently, using similar methods, they achieved a remarkable PCE of up to 20.04%, which is competitive with the corresponding

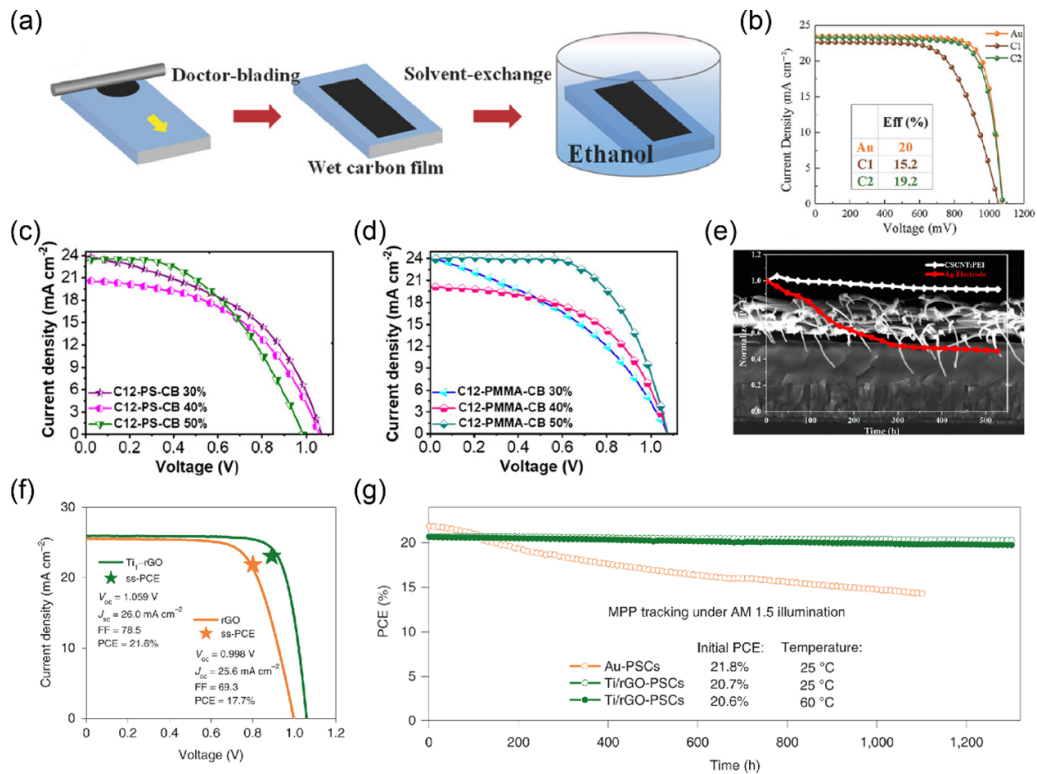


Figure 6. (a) Schematic illustration of the solvent-exchange method. [13] John Wiley & Sons. [© 2018 WILEY-VCH Verlag GmbH & Co. KGaA, Weinheim]. (b) Comparison of the performance based on different electrodes. [13] John Wiley & Sons. [© 2018 WILEY-VCH Verlag GmbH & Co. KGaA, Weinheim]. (c) and (d) Device performances based on different treated carbon electrodes. [94] John Wiley & Sons. [© 2020 WILEY-VCH Verlag GmbH & Co. KGaA, Weinheim]. (e) Cross-sectional SEM image of the carbon-electrode device and its stability compared to the Ag-electrode device [95]. Reprinted with permission from [95]. Copyright (2018) American Chemical Society. (f and g) PCE and stability enhancement of Ti/rGO-based CPSCs [15]. Reproduced from [15], with permission from Springer Nature.

metal-based PSCs [93]. Furthermore, the as-prepared devices exhibited excellent long-term stability, which retained 94% of its initial performance after storage for 1000 h at room temperature and 25% RH without encapsulation.

The properties of carbon pastes determine the performance of carbon electrodes in solar cells. Behrouznejad *et al* investigated how the weight ratio of carbon black to graphite and type of binder affect sheet resistance and resistivity of carbon composite layer, based on CuIn_{0.75}Ga_{0.25}S₂ HTL (figures 6(c) and (d)) [94]. The conductivity of the carbon composite layer with PMMA (4 wt.%) as a binder is significantly increased compared with that of PS (4 wt.%). They also found that the resistivity of deposited carbon layer increases by increasing the ratio of carbon black to carbon black plus graphite from 30% to 40% and 50%, but the FF of the prepared PSC is increased. They achieved the best efficiency of 15.9% in the champion cell, with J_{SC} of 23.86 mA cm⁻², V_{OC} of 1.08 V, and FF of 0.62. This efficiency is close to the best efficiency of the reference cell with conventional Spiro-OMeTAD/gold hole collector (16.3%) in this research.

In 2021, Zhang *et al* reported the application of reduced GO (rGO) as the back electrode in C-PSCs (figures 6(f) and (g)) [15]. They further tuned the electronic properties of rGO by anchoring single titanium (Ti) adatoms on it

in a well-defined Ti₁O₄-OH configuration. As a result, the series resistance of the carbon-based electrode was notably minimized. They achieved a steady-state PCE of up to 20.6% for CPSCs by combining with an advanced modular cell architecture, by stacking a semicell A (FTO/ETL/perovskite/spiro-OMeTAD/graphene) and charge collector B (FTO/graphene). Furthermore, the devices without encapsulation retained 98% and 95% of their initial PCEs for 1300 h under 1 sun continuous illumination at 25 °C and 60 °C, respectively.

As for the p-i-n device architecture, PCBM is commonly used as ETM. Because of its specific characteristics, PCBM cannot be replaced easily. Therefore, doping strategies and/or modification of PCBM have been carried out to improve the stability [96, 97]. However, challenge still exists when it comes to the fabrication of carbon electrodes on PCBM. Besides solvent destruction, energy-level alignment and interface compatibility are further two crucial problems. Zhou *et al* modified cross-stacked super-aligned carbon nanotube film on PCBM by employing polyethylenimine (PEI) (figure 6(e)) [95]. With a certain concentration of PEI (0.5 wt.%) doping, they achieved suitable energy-level alignment and promoted interfacial charge transfer, leading to a significant enhancement in the photovoltaic performance.

Finally, a maximum PCE of $\sim 11\%$ was obtained, with J_{SC} of 18.7 mA cm^{-2} , V_{OC} of 0.95 V , and FF of 0.61 . Moreover, the devices showed superior stability compared with Ag-electrode-based devices.

Up to now, few researchers focus on the development of new carbon-electrode materials, which are efficient, cheap, and environment friendly, while a lot of effort goes to under-layers. More work should be done in this field.

6. Summary and perspectives

CPSC based on the n-i-p structure has good commercial potential due to its high PCE, good stability, simple fabrication process, and low cost. In this paper, research progress on n-i-p CPSCs has been reviewed from the aspects of transporting/blocking layer design, interface engineering, perovskite layer regulation, and carbon-electrode modification.

The carrier recombination problem caused by the incompatibility between the traditional HTL material Spiro-OMeTAD and the commercial carbon paste in CPSCs makes the improvement of electron and hole extraction and transport become the basis of improving the PCE of CPSCs. Specifically, the following points can be considered in n-i-p structure CPSC.

- (i) As the condition that the traditional HTL side in CPSCs possesses poor transport capacity is hard to improve, optimization of the ETL side becomes essential. We can obtain the appropriate Fermi energy level of the transporting layer and the interface energy-level match, obtain higher carrier mobility, and better defect passivation effect through the selection and optimization of the ETL materials. Thus, we can get an excellent electron extraction and reduce the electron-hole recombination at the perovskite layer and interface.
- (ii) It is necessary to further explore HTL with great stability, high hole mobility, appropriate energy levels, and compatibility with the upper carbon electrode. Therefore, more innovative methods should be proposed, such as the development of a new HTL, the use of appropriate doping, the combination of double-layer HTL, and the introduction of interface protective layers.
- (iii) In addition to considering the use of ETL/HTL as the carrier transport medium, we can also consider introducing HBL/EBL at the corresponding position to block the unwanted carrier transport by the energy barrier to ensure the effective transport of another kind of carrier we want and reduce the carrier recombination inside the device.
- (iv) The interface between the upper and buried interfaces of perovskite and the transporting/blocking layer also has an important impact on carrier transport. Inserting an appropriate interface layer can play a very positive role, such as improving the crystallization quality of perovskite film, passivating interface defects, adjusting the arrangement of interfacial energy levels, introducing interfacial dipole layer, enhancing interfacial contact to

inhibit the occurrence of non-radiative recombination, and establishing carrier transport channels to accelerate the extraction and transfer of interfacial charges. Up to now, additives, such as organic salts, inorganic compounds, metal oxides, ionic liquids, fullerenes, SAMs, and organic polymers, are widely used in the interface layer.

When optimizing the perovskite layer in CPSCs, we should also take into account the special structure and properties of CPSCs. Because the carrier transport capacity of the electrode and transporting layer has intrinsic drawbacks, we should focus on achieving high-quality perovskite film to obtain good interfacial contact, long carrier lifetime, and strong carrier transport capacity, making up for the drawbacks of the overall device. We must precisely adjust the energy band structure of the perovskite surface to obtain a special energy-level matching suitable for CPSCs. We need to focus on exploring the production process with large area, low cost, high stability, and low energy consumption, and can be fabricated in the air to match the characteristics and application intention of the low-cost and simple manufacturing process of CPSCs to contribute to future commercial application.

The PCE of CPSC has exceeded 22% ; yet, a huge gap still exists compared with PSCs based on metal electrodes. The main causes of its low PCE is the intrinsic poor conductivity of the carbon electrode and the poor contact between the carbon electrode and the transporting layer. These drawbacks result in high contact resistance, which affects the transport and collection of carriers. We would like to highlight the following solutions to further enhance the performance of CPSCs: (a) develop new commercial carbon-electrode materials with high conductivity; (b) use strategies, such as interface modification, which may improve contact between the carbon electrode and the transporting layer; (c) achieve nondestructive contact between the carbon electrode and the transporting layer by hot-pressing or spraying method; (d) pay attention to the orientation of the spatial stacking of each layer of materials to obtain close stacking and efficient interfacial charge transfer; and (e) further develop large-area carbon-electrode deposition methods, such as blading or screen printing, to fabricate commercial modules of CPSCs.

In addition, it is necessary to further study the long-term stability of CPSCs and its influencing factors, while the matching encapsulation technology also awaits further improvement.

Acknowledgments

This study was financially supported by the National Natural Science Foundation of China (Nos. 61935016, 52173153, 62104059, 12174013, and 12074011), the National Key R&D Program of China (Nos. 2022YFB3606502 and 2022YFE0109000), the Natural Science Foundation of Hebei Province (F2021202044), and the Higher Education Science and Technology Research Project of Hebei Province (ZD2021031).

ORCID iDs

Wenjin Yu  <https://orcid.org/0000-0002-1301-4298>Yu Zou  <https://orcid.org/0000-0002-4413-1139>Cuncun Wu  <https://orcid.org/0000-0001-9178-3757>Lixin Xiao  <https://orcid.org/0000-0002-1190-6962>

References

- [1] Yoo J J *et al* 2021 Efficient perovskite solar cells via improved carrier management *Nature* **590** 587–93
- [2] Jeong J *et al* 2021 Pseudo-halide anion engineering for a-FAPbI₃ perovskite solar cells *Nature* **592** 381–5
- [3] Min H *et al* 2021 Perovskite solar cells with atomically coherent interlayers on SnO₂ electrodes *Nature* **598** 444–50
- [4] Kim M *et al* 2022 Conformal quantum dot-SnO₂ layers as electron transporters for efficient perovskite solar cells *Science* **375** 302–6
- [5] Liang L, Cai Y, Li X, Nazeeruddin M K and Gao P 2018 All that glitters is not gold: recent progress of alternative counter electrodes for perovskite solar cells *Nano Energy* **52** 211–38
- [6] Sirovinskaya S, Schmechel R and Benson N 2020 Influence of the cathode microstructure on the stability of inverted planar perovskite solar cells *RSC Adv.* **10** 23653–61
- [7] Kay A and Gratzel M 1996 Low cost photovoltaic modules based on dye sensitized nanocrystalline titanium dioxide and carbon powder *Sol. Energy Mater. Sol. Cells* **44** 99–117
- [8] Han H, Bach U, Cheng Y-B, Caruso R A and MacRae C 2009 A design for monolithic all-solid-state dye-sensitized solar cells with a platinized carbon counterelectrode *Appl. Phys. Lett.* **94** 103102
- [9] Mei A Y *et al* 2014 A hole-conductor-free, fully printable mesoscopic perovskite solar cell with high stability *Science* **345** 295–8
- [10] Zhang F G, Yang X C, Cheng M, Wang W H and Sun L C 2016 Boosting the efficiency and the stability of low cost perovskite solar cells by using CuPc nanorods as hole transport material and carbon as counter electrode *Nano Energy* **20** 108–16
- [11] Jeon I, Seo S, Sato Y, Delacou C, Anisimov A, Suenaga K, Kauppinen E I, Maruyama S and Matsuo Y 2017 Perovskite solar cells using carbon nanotubes both as cathode and as anode *J. Phys. Chem. C* **121** 25743–9
- [12] Wang Y *et al* 2022 Defective MWCNT enabled dual interface coupling for carbon-based perovskite solar cells with efficiency exceeding 22% *Adv. Funct. Mater.* **32** 2204831
- [13] Zhang H, Xiao J, Shi J, Su H, Luo Y, Li D, Wu H, Cheng Y-B and Meng Q 2018 Self-adhesive macroporous carbon electrodes for efficient and stable perovskite solar cells *Adv. Funct. Mater.* **28** 1802985
- [14] Zou Y *et al* 2021 Improving interfacial charge transfer by multi-functional additive for high-performance carbon-based perovskite solar cells *Appl. Phys. Lett.* **119** 151104
- [15] Zhang C *et al* 2021 Ti₁-graphene single-atom material for improved energy level alignment in perovskite solar cells *Nature Energy* **6** 1154–63
- [16] Lin S Y *et al* 2018 Efficient and stable planar hole-transport-material-free perovskite solar cells using low temperature processed SnO₂ as electron transport material *Org. Electron.* **53** 235–41
- [17] Wu Z, Song T and Sun B 2017 Carbon-based materials used for perovskite solar cells *Chemmanomat* **3** 75–88
- [18] Xu L *et al* 2017 Stable monolithic hole-conductor-free perovskite solar cells using TiO₂ nanoparticle binding carbon films *Org. Electron.* **45** 131–8
- [19] Zhang H, Wang H, Williams S T, Xiong D, Zhang W, Chueh -C-C, Chen W and Jen A K Y 2017 SrCl₂ derived perovskite facilitating a high efficiency of 16% in hole-conductor-free fully printable mesoscopic perovskite solar cells *Adv. Mater.* **29** 1606608
- [20] Liu X Y, Liu Z Y, Sun B, Tan X H, Ye H B, Tu Y X, Shi T L, Tang Z R and Liao G L 2018 17.46% efficient and highly stable carbon-based planar perovskite solar cells employing Ni-doped rutile TiO₂ as electron transport layer *Nano Energy* **50** 201–11
- [21] Liu X, Liu Z, Sun B, Tan X, Ye H, Tu Y, Shi T, Tang Z and Liao G 2018 All low-temperature processed carbon-based planar heterojunction perovskite solar cells employing Mg-doped rutile TiO₂ as electron transport layer *Electrochim. Acta* **283** 1115–24
- [22] Abulikemu M, Neophytou M, Barbe J M, Tietze M L, El Labban A, Anjum D H, Amassian A, McCulloch I and Del Gobbo S 2017 Microwave-synthesized tin oxide nanocrystals for low-temperature solution-processed planar junction organo-halide perovskite solar cells *J. Mater. Chem. A* **5** 7759–63
- [23] Baena J P C *et al* 2015 Highly efficient planar perovskite solar cells through band alignment engineering *Energy Environ. Sci.* **8** 2928–34
- [24] Ke W J *et al* 2015 Low-temperature solution-processed tin oxide as an alternative electron transporting layer for efficient perovskite solar cells *J. Am. Chem. Soc.* **137** 6730–3
- [25] Ye H B, Liu Z Y, Liu X Y, Sun B, Tan X H, Tu Y X, Shi T L, Tang Z R and Liao G L 2019 17.78% efficient low-temperature carbon-based planar perovskite solar cells using Zn-doped SnO₂ electron transport layer *Appl. Surf. Sci.* **478** 417–25
- [26] Khambunkoed N, Homnan S, Gardchareon A, Chattapiban N, Songsiririthigul P, Wongratanaphisan D and Ruankham P 2021 Fully-covered slot-die-coated ZnO thin films for reproducible carbon-based perovskite solar cells *Mater. Sci. Semicond. Process.* **136** 106151
- [27] Liu X, Tan X, Liu Z, Ye H, Sun B, Shi T, Tang Z and Liao G 2019 Boosting the efficiency of carbon-based planar CsPbBr₃ perovskite solar cells by a modified multistep spin-coating technique and interface engineering *Nano Energy* **56** 184–95
- [28] Liu Z Y, Sun B, Liu X, Han J, Ye H, Tu Y, Chen C, Shi T, Tang Z and Liao G 2018 15% efficient carbon based planar-heterojunction perovskite solar cells using a TiO₂/SnO₂ bilayer as the electron transport layer *J. Mater. Chem. A* **6** 7409–19
- [29] Liu Z Y, Liu X Y, Sun B, Tan X H, Ye H B, Tu Y X, Shi T L, Tang Z R and Liao G L 2019 Fully low-temperature processed carbon-based perovskite solar cells using thermally evaporated cadmium sulfide as efficient electron transport layer *Org. Electron.* **74** 152–60
- [30] Wu X, Xie L Q, Lin K B, Lu J X, Wang K X, Feng W J, Fan B B, Yin P G and Wei Z H 2019 Efficient and stable carbon-based perovskite solar cells enabled by the inorganic interface of CuSCN and carbon nanotubes *J. Mater. Chem. A* **7** 12236–43
- [31] Jin J J, Yang M, Deng W, Xin J, Tai Q, Qian J, Dong B, Li W, Wang J and Li J 2021 Highly efficient and stable carbon-based perovskite solar cells with the polymer hole transport layer *Sol. Energy* **220** 491–7
- [32] Zhao F, Zhou J, Tao J H, Guo Y X, Jiang J C and Chu J H 2022 Enhancing photovoltaic performance of carbon-based planar Cs₃Sb₂I_{9-x}Cl_x solar cells by using P3HT as hole transport material *J. Alloys Compd.* **897** 162741

- [33] Liu Z Y, Sun B, Liu X Y, Han J H, Ye H B, Shi T L, Tang Z R and Liao G L 2018 Efficient carbon-based CsPbBr₃ inorganic perovskite solar cells by using Cu-phthalocyanine as hole transport material *Nano Micro Lett.* **10** 34
- [34] Yang J L and Yan D H 2009 Weak epitaxy growth of organic semiconductor thin films *Chem. Soc. Rev.* **38** 2634–45
- [35] Duan J L, Wang Y D, Yang X Y and Tang Q W 2020 Alkyl-chain-regulated charge transfer in fluorescent inorganic CsPbBr₃ perovskite solar cells *Angew. Chem., Int. Ed.* **59** 4391–5
- [36] Duan J L, Zhao Y Y, Wang Y D, Yang X Y and Tang Q W 2019 Hole-boosted Cu(Cr,M)O₂ nanocrystals for all-inorganic CsPbBr₃ perovskite solar cells *Angew. Chem., Int. Ed.* **58** 16147–51
- [37] Yang F, Dong L R, Jang D, Saparov B, Tam K C, Zhang K C, Li N, Brabec C J and Egelhaaf H J 2021 Low temperature processed fully printed efficient planar structure carbon electrode perovskite solar cells and modules *Adv. Energy Mater.* **11** 2101219
- [38] Chu Q-Q *et al* 2019 Highly stable carbon-based perovskite solar cell with a record efficiency of over 18% via hole transport engineering *J. Mater. Sci. Technol.* **35** 987–93
- [39] Liu Y, He B L, Duan J L, Zhao Y Y, Ding Y, Tang M X, Chen H Y and Tang Q W 2019 Poly(3-hexylthiophene)/zinc phthalocyanine composites for advanced interface engineering of 10.03%-efficiency CsPbBr₃ perovskite solar cells *J. Mater. Chem. A* **7** 12635–44
- [40] Zong Z H, He B L, Zhu J W, Ding Y, Zhang W Y, Duan J L, Zhao Y Y, Chen H Y and Tang Q W 2020 Boosted hole extraction in all-inorganic CsPbBr₃ perovskite solar cells by interface engineering using MoO₂/N-doped carbon nanospheres composite *Sol. Energy Mater. Sol. Cells* **209** 110460
- [41] Mashhoun S, Hou Y, Chen H W, Tajabadi F, Taghavinia N, Egelhaaf H J and Brabec C J 2018 Resolving a critical instability in perovskite solar cells by designing a scalable and printable carbon based electrode-interface architecture *Adv. Energy Mater.* **8** 1802085
- [42] Zhong H *et al* 2022 All-inorganic perovskite solar cells with tetrabutylammonium acetate as the buffer layer between the SnO₂ electron transport film and CsPbI₃ *ACS Appl. Mater. Interfaces* **14** 5183–93
- [43] Cai W, Lv Y, Chen K, Zhang Z, Jin Y and Zhou X 2020 Carbon-based all-inorganic CsPbI₂Br perovskite solar cells using TiO₂ nanorod arrays: interface modification and the enhanced photovoltaic performance *Energy Fuels* **34** 11670–8
- [44] Ti J *et al* 2022 A “double-sided tape” modifier bridging the TiO₂/perovskite buried interface for efficient and stable all-inorganic perovskite solar cells *J. Mater. Chem. A* **10** 6649–61
- [45] Zhou Q, Duan J, Yang X, Duan Y and Tang Q 2020 Interfacial strain release from the WS₂/CsPbBr₃ van der Waals heterostructure for 1.7 V voltage all-inorganic perovskite solar cells *Angew. Chem., Int. Ed.* **59** 21997–2001
- [46] Deng F, Li X, Lv X, Zhou J, Chen Y, Sun X, Zheng Y-Z, Tao X and Chen J-F 2020 Low-temperature processing all-inorganic carbon-based perovskite solar cells up to 11.78% efficiency via alkali hydroxides interfacial engineering *ACS Appl. Energy Mater.* **3** 401–10
- [47] Zhu J, Tang M, He B, Zhang W, Li X, Gong Z, Chen H, Duan Y and Tang Q 2020 Improved charge extraction through interface engineering for 10.12% efficiency and stable CsPbBr₃ perovskite solar cells *J. Mater. Chem. A* **8** 20987–97
- [48] Yang Y *et al* 2019 An ultrathin ferroelectric perovskite oxide layer for high-performance hole transport material free carbon based halide perovskite solar cells *Adv. Funct. Mater.* **29** 1806506
- [49] Shi L *et al* 2021 MAAc ionic liquid-assisted defect passivation for efficient and stable CsPbIBr₂ perovskite solar cells *ACS Appl. Energy Mater.* **4** 10584–92
- [50] Zhang Z *et al* 2022 Accelerated sequential deposition reaction via crystal orientation engineering for low-temperature, high-efficiency carbon-electrode CsPbBr₃ solar cells *Energy Environ. Mater.* **e12524**
- [51] Liu L, Mei A, Liu T, Jiang P, Sheng Y, Zhang L and Han H 2015 Fully printable mesoscopic perovskite solar cells with organic silane self-assembled monolayer *J. Am. Chem. Soc.* **137** 1790–3
- [52] Chai W, Ma J, Zhu W, Chen D, Xi H, Zhang J, Zhang C and Hao Y 2021 Suppressing halide phase segregation in CsPbIBr₂ films by polymer modification for hysteresis-less all-inorganic perovskite solar cells *ACS Appl. Mater. Interfaces* **13** 2868–78
- [53] Yuan H, Zhao Y, Duan J, He B, Jiao Z and Tang Q 2018 Enhanced charge extraction by setting intermediate energy levels in all-inorganic CsPbBr₃ perovskite solar cells *Electrochim. Acta* **279** 84–90
- [54] Yang Y, Chen H, Hu C and Yang S 2019 Polyethyleneimine-functionalized carbon nanotubes as an interlayer to bridge perovskite/carbon for all inorganic carbon-based perovskite solar cells *J. Mater. Chem. A* **7** 22005–11
- [55] Li J, Yan F, Yang P, Duan Y, Duan J and Tang Q 2022 Suppressing interfacial shunt loss via functional polymer for performance improvement of lead-free Cs₂AgBiBr₆ double perovskite solar cells *Solar RRL* **6** 2100791
- [56] Ding Y, He B, Zhu J, Zhang W, Su G, Duan J, Zhao Y, Chen H and Tang Q 2019 Advanced modification of perovskite surfaces for defect passivation and efficient charge extraction in air-stable CsPbBr₃ perovskite solar cells *ACS Sustain. Chem. Eng.* **7** 19286–94
- [57] Wu Z, Liu Z, Hu Z, Hawash Z, Qiu L, Jiang Y, Ono L K and Qi Y 2019 Highly efficient and stable perovskite solar cells via modification of energy levels at the perovskite/carbon electrode interface *Adv. Mater.* **31** 1804284
- [58] Fu X, Zhou K, Zhou X, Ji H, Min Y and Qian Y 2022 Surface passivation for enhancing photovoltaic performance of carbon-based CsPbI₃ perovskite solar cells *J. Solid State Chem.* **308** 122891
- [59] Zhu W, Chai W, Chen D, Ma J, Chen D, Xi H, Zhang J, Zhang C and Hao Y 2021 High-efficiency (>14%) and air-stable carbon-based, all-inorganic CsPbI₂Br perovskite solar cells through a top-seeded growth strategy *ACS Energy Lett.* **6** 1500–10
- [60] Liu J, Zhou Q, Thein N K, Tian L, Jia D, Johansson E M J and Zhang X 2019 *In situ* growth of perovskite stacking layers for high-efficiency carbon-based hole conductor free perovskite solar cells *J. Mater. Chem. A* **7** 13777–86
- [61] Wu Y, Zhang Q, Fan L, Liu C, Wu M, Wang D and Zhang T 2021 Surface reconstruction-induced efficient CsPbI₂Br perovskite solar cell using phenylethylammonium iodide *ACS Appl. Energy Mater.* **4** 5583–9
- [62] Lee K, Kim J, Yu H, Lee J W, Yoon C-M, Kim S K and Jang J 2018 A highly stable and efficient carbon electrode-based perovskite solar cell achieved via interfacial growth of 2D PEA₂PbI₄ perovskite *J. Mater. Chem. A* **6** 24560–8
- [63] Zouhair S *et al* 2022 Employing 2D-perovskite as an electron blocking layer in highly efficient (18.5%) perovskite solar cells with printable low temperature carbon electrode *Adv. Energy Mater.* **12** 2200837
- [64] Wang K, Yin R, Sun W, Huo X, Liu J, Gao Y, You T and Yin P 2022 *In situ* constructing intermediate energy-level perovskite transition layer for 15.03% efficiency HTL-free carbon-based perovskite solar cells with a high fill factor of 0.81 *Solar RRL* **6** 2100647

- [65] Yu Z, Chen B, Liu P, Wang C, Bu C, Cheng N, Bai S, Yan Y and Zhao X 2016 Stable organic–inorganic perovskite solar cells without hole-conductor layer achieved via cell structure design and contact engineering *Adv. Funct. Mater.* **26** 4866–73
- [66] Mali S S, Kim H, Kim H H, Park G R, Shim S E and Hong C K 2017 Large area, waterproof, air stable and cost effective efficient perovskite solar cells through modified carbon hole extraction layer *Mater. Today Chem.* **4** 53–63
- [67] Wang H, Liu H, Dong Z, Song T, Li W, Zhu L, Bai Y and Chen H 2021 Size mismatch induces cation segregation in CsPbI₃: forming energy level gradient and 3D/2D heterojunction promotes the efficiency of carbon-based perovskite solar cells to over 15% *Nano Energy* **89** 106411
- [68] Han Q, Yang S, Wang L, Yu F, Cai X and Ma T 2022 A double perovskite participation for promoting stability and performance of carbon-based CsPbI₂Br perovskite solar cells *J. Colloid Interface Sci.* **606** 800–7
- [69] Ryu J, Lee K, Yun J, Yu H, Lee J and Jang J 2017 Paintable carbon-based perovskite solar cells with engineered perovskite/carbon interface using carbon nanotubes dripping method *Small* **13** 1701225
- [70] Wang Y, Zhao H, Mei Y, Liu H, Wang S and Li X 2019 Carbon nanotube bridging method for hole transport layer-free paintable carbon-based perovskite solar cells *ACS Appl. Mater. Interfaces* **11** 916–23
- [71] Wei H, Xiao J, Yang Y, Lv S, Shi J, Xu X, Dong J, Luo Y, Li D and Meng Q 2015 Free-standing flexible carbon electrode for highly efficient hole-conductor-free perovskite solar cells *Carbon* **93** 861–8
- [72] Guo Y, Zhao F, Tao J, Jiang J, Zhang J, Yang J, Hu Z and Chu J 2019 Efficient and hole-transporting-layer-free CsPbI₂Br planar heterojunction perovskite solar cells through rubidium passivation *ChemSusChem* **12** 983–9
- [73] Bai S, Cheng N, Yu Z, Liu P, Wang C and Zhao X-Z 2016 Cubic: column composite structure (NH₂CH=NH₂)_x(CH₃NH₃)_{1-x}PbI₃ for efficient hole-transport material-free and insulation layer free perovskite solar cells with high stability *Electrochim. Acta* **190** 775–9
- [74] Liang J, Liu Z, Qiu L, Hawash Z, Meng L, Wu Z, Jiang Y, Ono L K and Qi Y 2018 Enhancing optical, electronic, crystalline, and morphological properties of cesium lead halide by Mn substitution for high-stability all-inorganic perovskite solar cells with carbon electrodes *Adv. Energy Mater.* **8** 1800504
- [75] Chen H, Wei Z, He H, Zheng X, Wong K S and Yang S 2016 Solvent engineering boosts the efficiency of paintable carbon-based perovskite solar cells to beyond 14% *Adv. Energy Mater.* **6** 1502087
- [76] Chen H, Zheng X, Li Q, Yang Y, Xiao S, Hu C, Bai Y, Zhang T, Wong K S and Yang S 2016 An amorphous precursor route to the conformable oriented crystallization of CH₃NH₃PbBr₃ in mesoporous scaffolds: toward efficient and thermally stable carbon-based perovskite solar cells *J. Mater. Chem. A* **4** 12897–912
- [77] Zhang C, Luo Y, Chen X, Chen Y, Sun Z and Huang S 2016 Effective improvement of the photovoltaic performance of carbon-based perovskite solar cells by additional solvents *Nano Micro Lett.* **8** 347–57
- [78] Chang X *et al* 2016 Colloidal precursor-induced growth of ultra-even CH₃NH₃PbI₃ for high-performance paintable carbon-based perovskite solar cells *ACS Appl. Mater. Interfaces* **8** 30184–92
- [79] Liu C, He J, Wu M, Wu Y, Du P, Fan L, Zhang Q, Wang D and Zhang T 2020 All-inorganic CsPbI₂Br perovskite solar cell with open-circuit voltage over 1.3 V by balancing electron and hole transport *Solar RRL* **4** 2000016
- [80] Zhang C, Luo Q, Deng X, Zheng J, Ou-Yang W, Chen X and Huang S 2017 Enhanced efficiency and stability of carbon based perovskite solar cells using terephthalic acid additive *Electrochim. Acta* **258** 1262–72
- [81] Li L, Zhang R, Wu Z, Wang Y, Hong J, Rao H, Pan Z and Zhong X 2022 Crystallization control of air-processed wide-bandgap perovskite for carbon-based perovskite solar cells with 17.69% efficiency *Chem. Eng. J.* **n/a** 140566
- [82] Ullah S, Yang P, Wang J, Liu L, Yang S-E, Xia T and Chen Y 2022 Low-temperature processing of polyvinylpyrrolidone modified CsPbI₂Br perovskite films for high-performance solar cells *J. Solid State Chem.* **305** 122656
- [83] Liu J, Zhu L, Xiang S, Wei Y, Xie M, Liu H, Li W and Chen H 2019 Growing high-quality CsPbBr₃ by using porous CsPb₂Br₅ as an intermediate: a promising light absorber in carbon-based perovskite solar cells *Sustain. Energy Fuels* **3** 184–94
- [84] Li X, Zhang Y, Liu G, Zhang Z, Xiao L, Chen Z and Qu B 2021 Ionic liquid as an additive for two-step sequential deposition for air-processed efficient and stable carbon-based CsPbI₂Br all-inorganic perovskite solar cells *ACS Appl. Energy Mater.* **4** 13444–9
- [85] Yan J, Lin S, Qiu X, Chen H, Li K, Yuan Y, Long M, Yang B, Gao Y and Zhou C 2019 Accelerated hole-extraction in carbon-electrode based planar perovskite solar cells by moisture-assisted post-annealing *Appl. Phys. Lett.* **114** 103503
- [86] Zhang Q *et al* 2023 Suppressing “Coffee ring effect” to deposit high-quality CsPbI₃ perovskite films by drop casting *Chem. Eng. J.* **454** 140147
- [87] Zhang G, Zhang J, Yang Z, Pan Z, Rao H and Zhong X 2022 Role of moisture and oxygen in defect management and orderly oxidation boosting carbon-based CsPbI₂Br solar cells to a new record efficiency *Adv. Mater.* **34** 2206222
- [88] Liu L, Zuo C and Ding L 2021 Self-spreading produces highly efficient perovskite solar cells *Nano Energy* **90** 106509
- [89] Guo Y, Zhou J, Zhao F, Wu Y, Tao J, Zuo S, Jiang J, Hu Z and Chu J 2021 Carbon-based 2D-layered Rb_{0.15}Cs_{2.85}Sb₂Cl_xI_{9-x} solar cells with superior open-voltage up to 0.88 V *Nano Energy* **88** 106281
- [90] Tan X, Liu X, Liu Z, Sun B, Li J, Xi S, Shi T, Tang Z and Liao G 2020 Enhancing the optical, morphological and electronic properties of the solution-processed CsPbI₂Br₂ films by Li doping for efficient carbon-based perovskite solar cells *Appl. Surf. Sci.* **499** 143990
- [91] Liu X, Li J, Liu Z, Tan X, Sun B, Xi S, Shi T, Tang Z and Liao G 2020 Vapor-assisted deposition of CsPbI₂Br₂ films for highly efficient and stable carbon-based planar perovskite solar cells with superior V_{oc} *Electrochim. Acta* **330** 135266
- [92] Kroto H W, Heath J R, Obrien S C, Curl R F and Smalley R E 1985 C₆₀: buckminsterfullerene *Nature* **318** 162–3
- [93] Zhang H Y, Li Y, Tan S, Chen Z, Song K, Huang S, Shi J, Luo Y, Li D and Meng Q 2022 High-efficiency (>20%) planar carbon-based perovskite solar cells through device configuration engineering *J. Colloid Interface Sci.* **608** 3151–8
- [94] Behrouznejad F *et al* 2020 Effective carbon composite electrode for low-cost perovskite solar cell with inorganic CuIn_{0.75}Ga_{0.25}S₂ hole transport material *Solar RRL* **4** 1900564

- [95] Zhou Y *et al* 2018 Efficiently improving the stability of inverted perovskite solar cells by employing polyethylenimine-modified carbon nanotubes as electrodes *ACS Appl. Mater. Interfaces* **10** 31384–93
- [96] Seo J, Park S, Kim Y C, Jeon N J, Noh J H, Yoon S C and Seok S I 2014 Benefits of very thin PCBM and LiF layers for solution-processed p-i-n perovskite solar cells *Energy Environ. Sci.* **7** 2642–6
- [97] Babu V, Pineda R F, Ahmad T, Alvarez A O, Castriotta L A, Di Carlo A, Fabregat-Santiago F and Wojciechowski K 2020 Improved stability of inverted and flexible perovskite solar cells with carbon electrode *ACS Appl. Energy Mater.* **3** 5126–34